LETTER

https://doi.org/10.1038/s41586-018-0054-x

Rapid energy-efficient manufacturing of polymers and composites via frontal polymerization

Ian D. Robertson[1,2,7], Mostafa Yourdkhani[1,7], Polette J. Centellas[1,3], Jia En Aw[1,3], Douglas G. Ivanoff[1,4], Elyas Goli[1,5], Evan M. Lloyd[1,6], Leon M. Dean[1,4], Nancy R. Sottos[1,4], Philippe H. Geubelle[1,3], Jeffrey S. Moore[1,2] & Scott R. White[1,3]*

Thermoset polymers and composite materials are integral to today's aerospace, automotive, marine and energy industries and will be vital to the next generation of lightweight, energy-efficient structures in these enterprises, owing to their excellent specific stiffness and strength, thermal stability and chemical resistance[1–5]. The manufacture of high-performance thermoset components requires the monomer to be cured at high temperatures (around 180 °C) for several hours, under a combined external pressure and internal vacuum[6]. Curing is generally accomplished using large autoclaves or ovens that scale in size with the component. Hence this traditional curing approach is slow, requires a large amount of energy and involves substantial capital investment[6,7]. Frontal polymerization is a promising alternative curing strategy, in which a self-propagating exothermic reaction wave transforms liquid monomers to fully cured polymers. We report here the frontal polymerization of a high-performance thermoset polymer that allows the rapid fabrication of parts with microscale features, three-dimensional printed structures and carbon-fibre-reinforced polymer composites. Precise control of the polymerization kinetics at both ambient and elevated temperatures allows stable monomer solutions to transform into fully cured polymers within seconds, reducing energy requirements and cure times by several orders of magnitude compared with conventional oven or autoclave curing approaches. The resulting polymer and composite parts possess similar mechanical properties to those cured conventionally. This curing strategy greatly improves the efficiency of manufacturing of high-performance polymers and composites, and is widely applicable to many industries.

Present technologies for manufacturing high-performance thermoset and fibre-reinforced polymer composite (FRPC) parts rely on curing in large, expensive autoclaves or ovens. For example, curing a small section of the Boeing 787's carbon fibre/epoxy fuselage is estimated to require 350 gigajoules (GJ) of energy during its eight-hour cure cycle, producing more than 80 tons of carbon dioxide[7]. Consequently, there has been much interest in producing these materials with less energy, reducing their cost and environmental impact and furthering their application in commercial markets[6,8–11]. Frontal polymerization is a promising curing strategy that substantially reduces manufacturing burdens by using the enthalpy of polymerization to provide the energy for materials synthesis, rather than requiring an external energy source[12]. In frontal polymerization, a solution of a monomer and a latent initiator is heated locally until the initiator is activated for polymerization of the monomer, producing heat from the polymerization that further drives the reaction. The autoactivation process produces a propagating reaction wave that rapidly transforms the available monomer into polymer. Frontal polymerization has been used to synthesize a variety of polymeric materials, including functionally graded polymers, nanocomposites, hydrogels, sensory materials and FRPCs[13–21]. Most of the materials used in frontal polymerization to date, however, are unsuitable for high-performance applications. For example, although acrylate monomers possess the requisite energy density and reactivity to frontally polymerize, the mechanical properties of the resulting polymers are greatly inferior to those used in structural FRPCs. By contrast, epoxy monomers produce mechanically robust polymers, but are challenging to frontally polymerize because of their lower reactivity[20,22]. Moreover, it is essential for successful manufacturing of FRPCs that the liquid monomer be stable and essentially free of background polymerization at room temperature. These requirements motivate the development of frontal-polymerization chemistry with a controllable and stable processing window, a high energy density and reactivity, and a mechanically and thermally robust polymer product.

Here, we demonstrate that well-controlled frontal polymerization facilitates the rapid production of high-performance thermoset and FRPC parts with minimal energy input. Furthermore, the process is compatible with commonly used manufacturing techniques and produces high-quality thermoset materials. Frontal curing of FRPCs is challenging because a high volume fraction of fibres is necessary to produce a composite material with good mechanical properties, yet the corresponding reduction in resin content reduces the exothermic energy density available for frontal polymerization. As such, the frontal-polymerization chemistry must have a high molar enthalpy of polymerization and sufficiently high rate of polymerization to prevent frontal quenching. Fabricating small components with frontal polymerization is similarly challenging because much of the heat of polymerization is lost to the environment through air or tooling surfaces[23,24].

The frontal ring-opening metathesis polymerization (FROMP) of dicyclopentadiene (DCPD) using a thermally activated ruthenium catalyst exhibits the high energy density, high reactivity and low viscosity required for the synthesis of high-performance thermosets (Fig. 1a). The resulting polydicyclopentadiene (pDCPD) is a crosslinked thermoset polymer that is suitable for the fabrication of durable resin and FRPC parts, owing to its high fracture toughness, impact resistance, stiffness and chemical resistance[25–27]. However, FROMP chemistry has been severely limited in the past by its short pot life of less than 30 minutes[28,29]. Recently, we demonstrated that inhibitors of the alkyl phosphite family substantially extend the room-temperature liquid-processing window for FROMP of DCPD up to 30 hours[30]. Here, we use phosphite-inhibited FROMP of DCPD to efficiently fabricate neat pDCPD and carbon FRPC structures. Compared with conventional curing, our frontal-polymerization strategy reduces energy requirements by more than ten orders of magnitude for large components (Fig. 1b).

Phosphite-inhibited DCPD containing second-generation Grubbs' catalyst (GC2) slowly transforms at room temperature from a liquid to a viscoelastic gel. Remarkably, the gelation of the monomer does not result in concomitant spontaneous polymerization, as observed with previous FROMP chemistries. Tuning the inhibitor concentration allows access to a range of rheological profiles between the low-viscosity

[1]Beckman Institute for Advanced Science and Technology, University of Illinois at Urbana-Champaign, Urbana, IL, USA. [2]Department of Chemistry, University of Illinois at Urbana-Champaign, Urbana, IL, USA. [3]Department of Aerospace Engineering, University of Illinois at Urbana-Champaign, Urbana, IL, USA. [4]Department of Materials Science and Engineering, University of Illinois at Urbana-Champaign, Urbana, IL, USA. [5]Department of Civil and Environmental Engineering, University of Illinois at Urbana-Champaign, Urbana, IL, USA. [6]Department of Chemical and Biomolecular Engineering, University of Illinois at Urbana-Champaign, Urbana, IL, USA. [7]These authors contributed equally: Ian D. Robertson, Mostafa Yourdkhani. *e-mail: swhite@illinois.edu

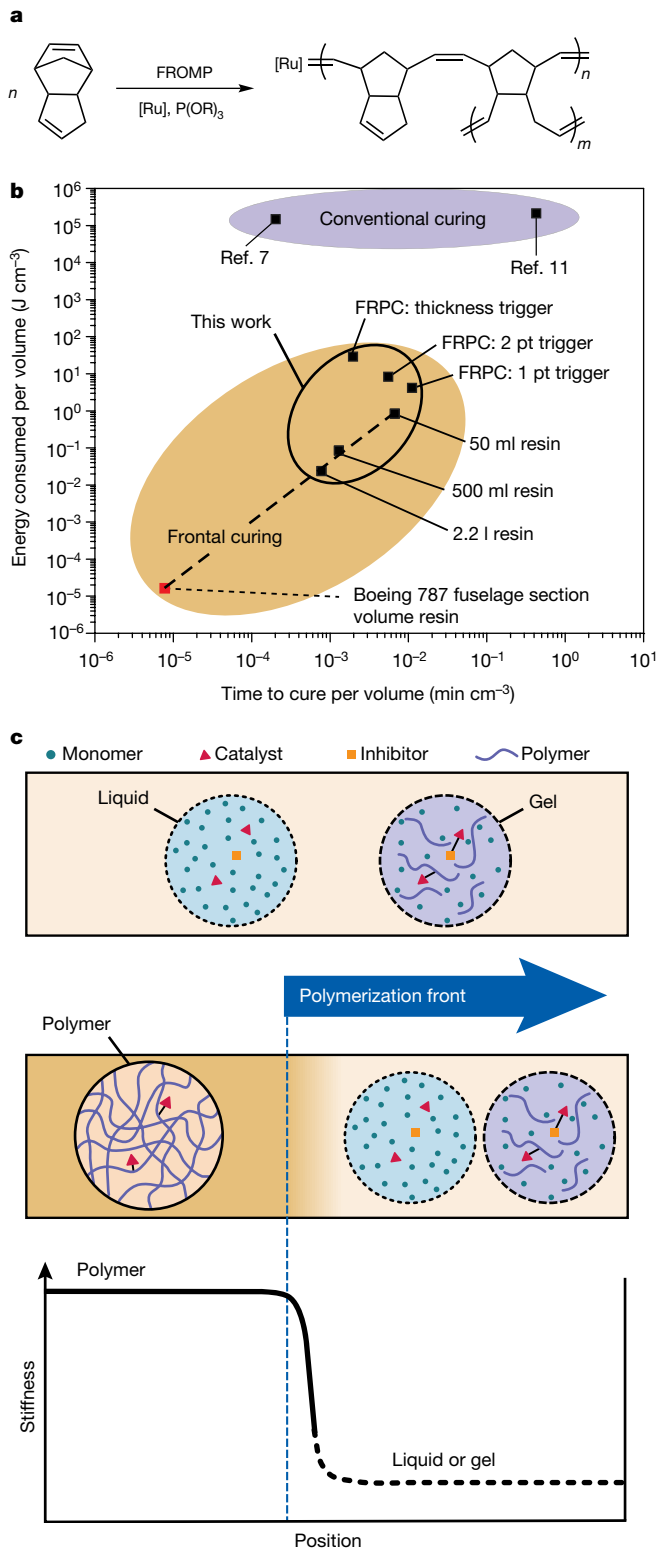

Fig. 1 | Overview of the frontal-polymerization concept. a, Scheme for the FROMP of DCPD using a ruthenium catalyst (Ru; that is, second-generation Grubbs' catalyst) and an alkyl phosphite inhibitor ($P(OR)_3$). **b**, Comparison of the energy required for curing versus the time taken for curing via frontal polymerization and conventional curing. Given that the only energy needed for frontal curing is the initiating stimulus, the process requires several orders of magnitude less energy than conventional curing, while also occurring faster and with less expensive equipment. References 7 and 11 describe the manufacturing of a section of the Boeing 787 fuselage and a 900 cm^2 carbon FRPC panel, respectively. We calculated that the curing of a section of the Boeing 787 fuselage by FROMP (red square) reduces the energy consumption by ten orders of magnitude compared with conventional techniques. **c**, In the technique used here, the FROMP solution is triggered to polymerize in its liquid stage, or allowed to form a gel at room temperature and later activated. In both cases, a rapid FROMP reaction transforms the liquid or gel into a durable thermoset polymer.

liquid and free-standing elastomeric gel, all of which frontally polymerize upon thermal activation (Fig. 1c). These free-standing gels are deformable and easily embossed; the resulting patterned gel structure can be quickly fixed into a rigid pDCPD structure via FROMP (Fig. 2a–c and Supplementary Video 1). Moreover, when the liquid monomer is poured onto a micropatterned substrate, peeled off in the gel stage, and polymerized by FROMP, a high-fidelity replica is produced in one step (Fig. 2d, e).

The gel is amenable to three-dimensional (3D) printing during the high-viscosity fluid stage, whereby the viscous liquid is extruded from a print head and frontally polymerized immediately upon exiting the nozzle, allowing for the simultaneous free-form printing and curing of thermoset polymers (Fig. 2f and Supplementary Video 2). Matching the print-head velocity to the front velocity allows for the manufacture of free-form complex architectures that are not possible with traditional additive manufacturing approaches (Fig. 2g, h). Once printing is complete, the part is fully cured (Extended Data Fig. 1c) and there is no need for further processing.

In marked contrast with traditional autoclave processing, we can fabricate FRPC parts in less than 5 minutes through FROMP of woven carbon fibres infused with the monomer solution (Fig. 2i, j). The very low viscosity of the liquid monomer at room temperature (~1.5 cP) allows the resin to be rapidly infused into continuous-fibre layups that have a high volume fraction of fibres via out-of-autoclave processing techniques such as vacuum-assisted resin-transfer moulding (VARTM). FROMP is triggered by briefly powering a resistive heating wire embedded in the layup, which provides sufficient thermoelectric stimulus (Fig. 3a and Supplementary Video 3). The high reactivity of DCPD facilitates FROMP in thin FRPC laminates with up to 50 vol% fibre reinforcement, while remarkably reducing the manufacturing time and required energy. We can further reduce the manufacturing time by using multiple triggering points (Fig. 3b and Supplementary Video 4) or by propagating the reaction through the thickness using a resistive heater underneath the layup (Fig. 3c and Supplementary Video 5). However, commensurately more triggering energy is required in these configurations (Fig. 3a–c). We expected the relatively low volume fraction of monomers in the FRPCs to reduce the frontal velocity. Surprisingly, however, the frontal velocity in the FROMP-FRPC (9.8 cm min^{-1}) was higher than that observed in neat resin for the same formulation (7.5 cm min^{-1}). We surmise that the carbon fibre conducts heat from the exothermic reaction and preheats a region of monomer ahead of the front, accelerating the reaction and producing a higher frontal velocity.

Numerical simulation of a carbon-fibre bundle, or tow, in the resin supports this hypothesis. Using a simple model system—which consists of a single carbon-fibre tow made of 3,000 individual fibres suspended in neat resin—we observe that the carbon fibres accelerate FROMP and produce a distinct change in the front shape from flat to conical (Fig. 3d, e). To provide analytical insight, we carried out numerical simulations of the thermochemical problem using a transient, nonlinear finite-element solver. We used an adaptive meshing scheme to capture the sharp gradients in temperature and degree of cure in the immediate vicinity of the propagating polymerization front. As shown by the computed thermal solutions in Fig. 3d, e, the higher thermal conductivity of the fibre tow changes the thermal field ahead of the front, thereby modifying the shape and speed of the front. The numerical solver provides useful insights into FROMP by creating a direct link between the cure kinetics model and FROMP propagation. For example, simulations of multipoint initiation predict a temperature spike upon front convergence, because the heat of reaction is no longer

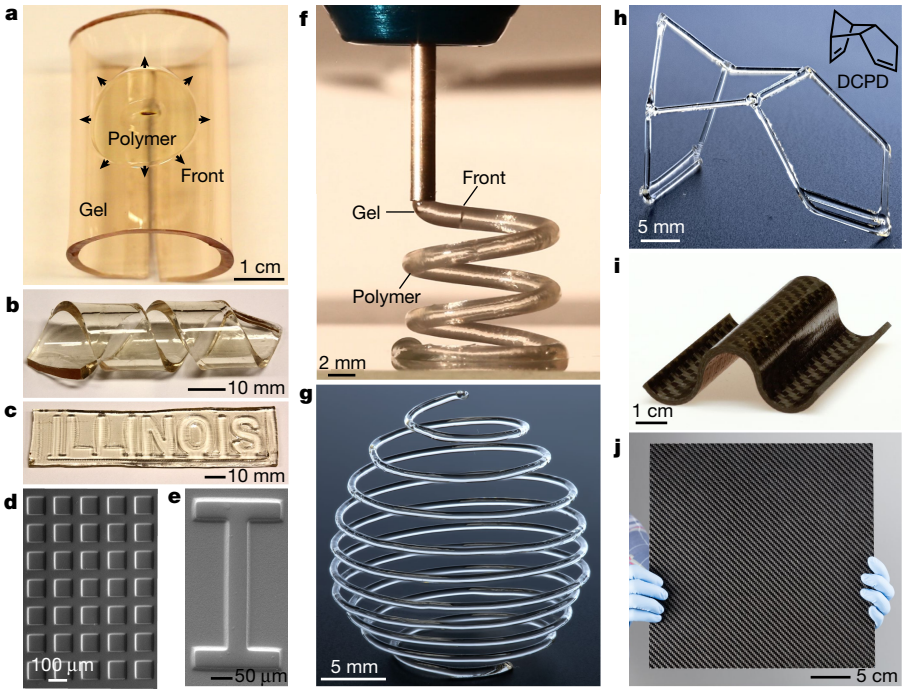

Fig. 2 | Advanced manufacturing with FROMP. a, FROMP in a free-standing gel, propagating radially from a single initiation-point source. **b**–**e**, Macropatterned/micropatterned pDCPD produced by gel FROMP. In **b**, a flat gel sheet is rolled into a helix structure before FROMP. In **c**, a flat gel sheet is imprinted with an ILLINOIS stamp before FROMP. In **d** and **e**, gel sheets are produced by moulding at room temperature for 18 hours and followed by FROMP to solidify the micropattern. **f**, 3D printing of gel DCPD solution that is solidified by FROMP immediately following extrusion from the print head. **g**, **h**, Free-form 3D-printed structures produced via FROMP. **i**, A corrugated carbon FRPC part fabricated by FROMP using vacuum-assisted resin-transfer moulding. **j**, A 900 cm^2 carbon FRPC panel (with 51% fibre volume fraction) cured by FROMP in 5 minutes using about 750 J of energy.

conducted away from the front. This thermal overshoot is observed in two-point initiation experiments (Fig. 3b), and, if excessive, may lead to material degradation near the location of merging fronts. Optimization strategies for the manufacture of FRPCs with minimum curing time and required energy coupled with high quality will require similar computational modelling approaches.

Carefully selecting the phosphite inhibitor and its concentration enables us to control room-temperature rheological profiles as well as frontal velocity (Fig. 4a). Figure 4b divides the rheological characteristics of a particular formulation into three regimes. Prior to the gel point, liquid FROMP is suitable for a wide variety of infusion techniques that require a low-viscosity resin. After the gel point, the material exhibits increased

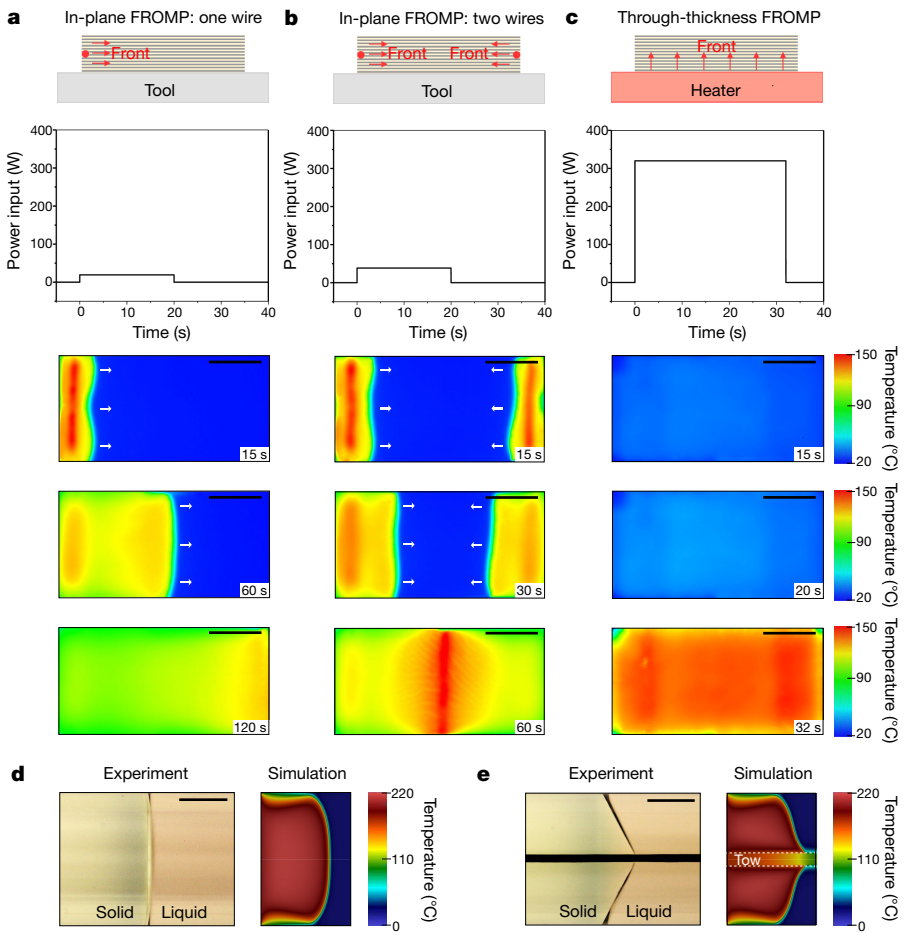

Fig. 3 | Composite fabrication and modelling. The FROMP curing of FRPC is a versatile process. **a**, Heating one embedded wire ignites a single front that propagates (left to right) to fully cure the FRPC in about 2 minutes. **b**, Heating two embedded wires (opposite ends) ignites two fronts that merge in the middle, completing curing in half the time (about 1 minute). **c**, Heating the layup from below ignites a front that travels through the thickness of the panel and completes the cure in about 30 seconds. Still images are captured using a thermal infrared camera. Scale bar in **a**–**c** represents 5 cm. **d**, A propagating FROMP reaction wave captured experimentally and via simulation. The optical difference between the solid and liquid phases shows that the front shape is slightly convex in the direction of propagation (left to right). This frontal shape is closely matched by simulation. **e**, In the presence of a single carbon-fibre tow, the frontal shape is altered and the front is accelerated near the tow surface. The increase in front speed from **d** to **e** is roughly 10%. Scale bar in **d**, **e** represents 4 mm.

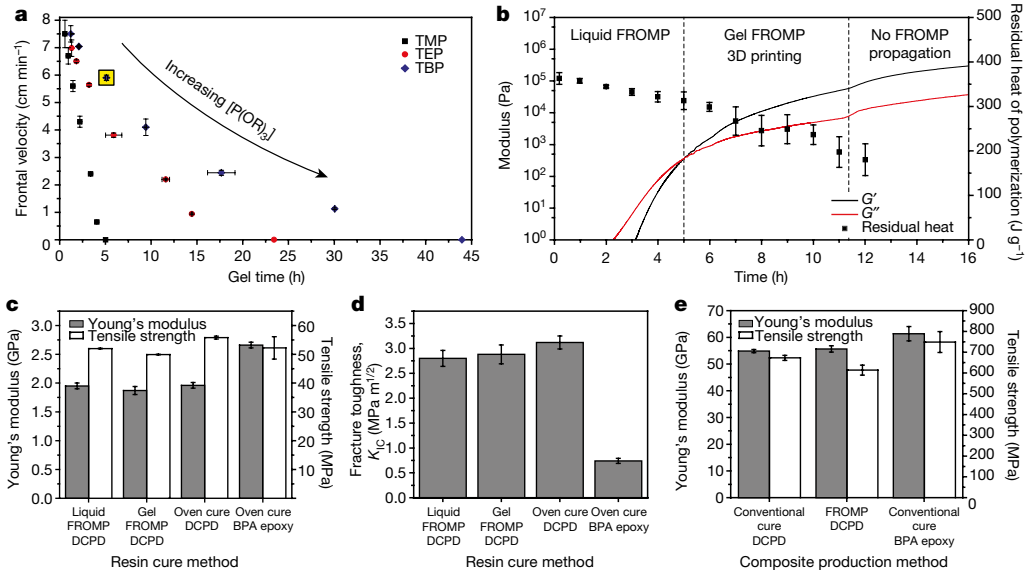

Fig. 4 | Characterization of the FROMP curing approach. a, Gel time and frontal velocity are controlled by the identity of the phosphite inhibitor (TMP, trimethyl phosphite; TEP, triethyl phosphite; TBP, tributyl phosphite) and its concentration (0.3, 0.5, 1, 2, 4 or 8 molar equivalents with respect to GC2 catalyst). FROMP is no longer observed with 9, 12 or 14 molar equivalents of TMP, TEP and TBP, respectively. Error bars represent standard deviation from the mean ($n = 3$). **b**, Representative rheological and thermal behaviour for curing at room temperature (23 °C) of a FROMP solution containing 1 molar equivalent TBP inhibitor with respect to GC2 catalyst (highlighted yellow data point in **a**), showing three rheological regimes. The liquid FROMP stage is suitable for resin-infusion/transfer manufacturing. After gelation, both 3D printing and the macropatterning/micropatterning of gels are possible. After vitrification, FROMP is no longer possible. The residual heat at each stage is determined by DSC analysis. The initial data point at $t = 0.19$ hours indicates the total enthalpy of the reaction of dicyclopentadiene ($H_r = 362.8 \pm 13.1$ J g^{-1}). Error bars represent standard deviation from the mean ($n = 3$). G', storage modulus; G'', loss modulus. **c**, Young's modulus and tensile strength for liquid FROMP, gel FROMP, and oven-cured pDCPD. A bisphenol A (BPA) aerospace-grade epoxy is shown for comparison. Error bars represent standard deviation from the mean ($n = 7$). **d**, Mode I fracture toughness (K_{IC}, where K is the stress intensity factor, I denotes 'mode I crack opening', and C denotes 'critical') for liquid FROMP ($n = 5$), gel FROMP ($n = 5$) and oven-cured pDCPD ($n = 6$) in comparison with BPA aerospace-grade epoxy ($n = 8$). Error bars represent standard deviation from the mean. **e**, Young's modulus and tensile strength for conventional-cured (51% volume fraction; $n = 10$) and FROMP-cured (51% volume fraction; $n = 13$) pDCPD-FRPCs in comparison with aerospace-grade (BPA) carbon/epoxy FRPC (52% volume fraction; $n = 8$). Error bars represent standard deviation from the mean.

elasticity, enabling access to additional processing techniques. During the first part of the post-gelation regime, the monomer solution is a viscous liquid suitable for 3D printing (vide supra). It exhibits shear thinning behaviour (Extended Data Fig. 1d) and is readily extruded from a print head under pressure. In the latter stages of this regime, the material forms a free-standing gel that is resistant to plastic flow. This stage is useful for casting micropatterns and imprinting (vide supra). The regime ends with a secondary vitrification transition that corresponds to the point at which there is no longer sufficient chemical energy in the reactive formulation to sustain FROMP. For larger concentrations of tributyl phosphite (TBP), this transition occurs more than 40 hours after mixing at 23 °C, providing sufficient time for manufacturing. For stiff gel applications, a trimethyl phosphite (TMP) formulation that gels quickly may be desirable. For 3D printing and composite manufacturing, a longer processing window is desired; therefore, TBP or triethyl phosphite (TEP) should be used at the highest concentration that still enables FROMP.

We monitored the residual exotherm by differential scanning calorimetry (DSC) during room-temperature curing, to examine the effect of gelation on the cure profile and to correlate the rheological transitions with the degree of cure (Fig. 4b). We found that there is a slight shift of the exothermic peak to lower temperatures as the curing proceeds, and that the peak broadens substantially (Extended Data Fig. 1a). This behaviour suggests that the reactive formulation becomes more sensitive to increases in temperature during gelation; this sensitivity facilitates frontal polymerization in the partially cured state. The increase in reactivity may result from the formation of new catalyst species in situ, as seen in ^{31}P nuclear magnetic resonance (NMR) spectroscopy of the gelled material[30]. The pDCPD produced after both liquid and gel FROMP exhibits a minimal residual exotherm, indicating that a complete cure is achieved (Extended Data Fig. 1b).

FROMP-cured pDCPD exhibits comparable mechanical properties to conventionally (oven) cured pDCPD. The tensile strength and stiffness of pDCPD that has been frontally polymerized from both the liquid and the gel stage indicate that frontal polymerization provides the energy necessary for complete cross-linking of the monomer (Fig. 4c). Comparing the tensile properties of pDCPD with those of an aerospace-grade bisphenol A (BPA) epoxy system indicates that this new curing strategy and matrix resin produce polymers suitable for use in high-performance applications. In fact, the enhanced fracture toughness of FROMP-pDCPD compared with BPA epoxy (Fig. 4d) may provide high-performance composites with superior energy absorption and fatigue resistance[27].

Frontally polymerized FRPCs also exhibit mechanical properties comparable to those of FRPCs manufactured using a conventional aerospace-grade BPA epoxy system (Fig. 4e). The carbon fibre used in our FRPCs was surface-treated to allow interaction with epoxy functional groups; we envisage that greater tensile properties for pDCPD-FRPCs should be made possible by tailoring the interfacial interaction of the carbon fibre and pDCPD through proper fibre surface treatments. We attribute the slightly lower tensile strength of FROMP-cured compared with conventionally cured pDCPD composite specimens to the lower degree of cross-linking, resulting from heat loss through the fibre reinforcement and tooling (Extended Data Table 2).

In conclusion, we have developed and demonstrated a new frontal polymerization curing method for the rapid, energy-efficient manufacturing of thermoset pDCPD and FRPCs. This method is applicable to moulding, imprinting, 3D printing and resin-infusion techniques, and the resulting polymers and carbon-fibre-reinforced polymer composites exhibit excellent mechanical properties, comparable to those of materials produced by conventional techniques. We envisage that the controlled frontal polymerization of high-quality resins will

enable a variety of new manufacturing technologies—such as on-site, on-demand manufacturing, in-the-field repair of FRPCs and mould-less production—owing to the spatiotemporal control over the curing process.

Online content

Any Methods, including any statements of data availability and Nature Research reporting summaries, along with any additional references and Source Data files, are available in the online version of the paper at https://doi.org/10.1038/s41586-018-0054-x.

Received: 5 December 2017; Accepted: 19 February 2018;
Published online 9 May 2018.

1. Pascault, J.-P., Sautereau, H., Verdu, J. & Williams, R. J. J. *Thermosetting Polymers* (CRC Press, New York, 2002).
2. Daniel, I. M. & Ishai, O. *Engineering Mechanics of Composite Materials* (Oxford Univ. Press, Oxford, 2005).
3. Brøndsted, P., Lilholt, H. & Lystrup, A. Composite materials for wind power turbine blades. *Annu. Rev. Mater. Res.* **35**, 505–538 (2005).
4. Friedrich, K. & Almajid, A. A. Manufacturing aspects of advanced polymer composites for automotive applications. *Appl. Compos. Mater.* **20**, 107–128 (2013).
5. Karbhari, V. M. & Seible, F. Fiber reinforced composites—advanced materials for the renewal of civil infrastructure. *Appl. Compos. Mater.* **7**, 95–124 (2000).
6. Abliz, D. et al. Curing methods for advanced polymer composites—a review. *Polym. Polymer Compos.* **21**, 341–348 (2013).
7. Timmis, A. J. et al. Environmental impact assessment of aviation emission reduction through the implementation of composite materials. *Int. J. Life Cycle Assess.* **20**, 233–243 (2015).
8. Taynton, P. et al. Repairable woven carbon fiber composites with full recyclability enabled by malleable polyimine networks. *Adv. Mater.* **28**, 2904–2909 (2016).
9. Lee, J., Stein, I. Y., Kessler, S. S. & Wardle, B. L. Aligned carbon nanotube film enables thermally induced state transformations in layered polymeric materials. *ACS Appl. Mater. Interfaces* **7**, 8900–8905 (2015).
10. Li, N., Li, Y., Hang, X. & Gao, J. Analysis and optimization of temperature distribution in carbon fiber reinforced composite materials during microwave curing process. *J. Mater. Process. Technol.* **214**, 544–550 (2014).
11. Witik, R. A. et al. Economic and environmental assessment of alternative production methods for composite aircraft components. *J. Clean. Prod.* **29–30**, 91–102 (2012).
12. Pojman, J. A. in *Polymer Science: A Comprehensive Reference* Vol. 4 (eds. Matyjaszewski, K. & Möller, M.) 957–980 (Elsevier, Amsterdam, 2012).
13. Chekanov, Y. A. & Pojman, J. A. Preparation of functionally gradient materials via frontal polymerization. *J. Appl. Polym. Sci.* **78**, 2398–2404 (2000).
14. Nuvoli, D. et al. Synthesis and characterization of functionally gradient materials obtained by frontal polymerization. *ACS Appl. Mater. Interfaces* **7**, 3600–3606 (2015).
15. Chen, S., Sui, J., Chen, L. & Pojman, J. A. Polyurethane–nanosilica hybrid nanocomposites synthesized by frontal polymerization. *J. Polym. Sci. A* **43**, 1670–1680 (2005).
16. Yan, Q.-Z., Zhang, W.-F., Lu, G.-D., Su, X.-T. & Ge, C.-C. Frontal polymerization synthesis of starch-grafted hydrogels: effect of temperature and tube size on propagating front and properties of hydrogels. *Chem. Eur. J.* **12**, 3303–3309 (2006).
17. Guo, X., Wang, C.-F., Fang, Y., Chen, L. & Chen, S. Fast synthesis of versatile nanocrystal-embedded hydrogels toward the sensing of heavy metal ions and organoamines. *J. Mater. Chem.* **21**, 1124–1129 (2011).
18. Sanna, R. et al. Polymer hydrogels of 2-hydroxyethyl acrylate and acrylic acid obtained by frontal polymerization. *J. Polym. Sci. A* **50**, 1515–1520 (2012).
19. Nagy, I. P., Sike, L. & Pojman, J. A. Thermochromic composite prepared via a propagating polymerization front. *J. Am. Chem. Soc.* **117**, 3611–3612 (1995).
20. White, S. R. & Kim, C. A simultaneous lay-up and in situ cure process for thick composites. *J. Reinf. Plast. Compos.* **12**, 520–535 (1993).
21. Kim, C., Teng, H., Tucker, C. L. & White, S. R. The continuous cuing process for thermoset polymer composites. Part 1: modeling and demonstration. *J. Compos. Mater.* **29**, 1222–1253 (1995).
22. Scognamillo, S., Bounds, C., Luger, M., Mariani, A. & Pojman, J. A. Frontal cationic curing of epoxy resins. *J. Polym. Sci. A* **48**, 2000–2005 (2010).
23. Robertson, I. D., Lopez Hernandez, H., White, S. R. & Moore, S. Rapid stiffening of a microfluidic endoskeleton via frontal polymerization. *ACS Appl. Mater. Interfaces* **6**, 18469–18474 (2014).
24. Datta, P., Efimenko, K. & Genzer, J. The effect of confinement on thermal frontal polymerization. *Polym. Chem.* **3**, 3243–3246 (2012).
25. Delaude, L. & Noels, A. F. in *Kirk-Othmer Encyclopedia of Chemical Technology* Vol. 26 (ed. Seidel, A.) 920–958 (John Wiley & Sons, Inc., Malden, 2007).
26. Woodson, C. S. Jr & Grubbs, R. H. Polymeric composites including dicyclopentadiene and related monomers. US patent 6,310,121 B1 (2001).
27. Vallons, K. A. M., Drozdzak, R., Charret, M., Lomov, S. V. & Verpoest, I. Assessment of the mechanical behaviour of glass fibre composites with a tough polydicyclopentadiene (PDCPD) matrix. *Compos. Part A Appl. Sci. Manuf.* **78**, 191–200 (2015).
28. Mariani, A., Fiori, S., Chekanov, Y. & Pojman, J. A. Frontal ring-opening metathesis polymerization of dicyclopentadiene. *Macromolecules* **34**, 6539–6541 (2001).
29. Ruiu, A., Sanna, D., Alzari, V., Nuvoli, D. & Mariani, A. Advances in the frontal ring opening metathesis polymerization of dicyclopentadiene. *J. Polym. Sci. A* **52**, 2776–2780 (2014).
30. Robertson, I. D. et al. Alkyl phosphite inhibitors for frontal ring-opening metathesis polymerization greatly increase pot life. *ACS Macro Lett.* **6**, 609–612 (2017).

Acknowledgements This research was conducted as part of the Center for Excellence for Self-Healing, Regeneration and Structural Remodeling, supported by the United States Air Force Office of Scientific Research through award FA9550-16-1-0017. We thank J. Sung for preparing the micropatterned silicon substrates, T. Ross for sample photography, D. Loudermilk for graphics assistance, and the Beckman Institute for Advanced Science and Technology for use of their facilities and equipment. I.D.R. thanks the US Department of Defense for a National Defense Science and Engineering Graduate Fellowship. L.M.D. thanks the National Science Foundation for a Graduate Research Fellowship.

Reviewer information *Nature* thanks J. Pojman and the other anonymous reviewer(s) for their contribution to the peer review of this work.

Author contributions S.R.W., J.S.M., N.R.S. and P.H.G. directed the research. J.S.M., S.R.W., N.R.S. and I.D.R. conceived the idea. I.D.R., M.Y., P.J.C., J.E.A., D.G.I., E.M.L. and L.M.D. performed the experiments. E.G. conducted the computational studies. All authors participated in writing the manuscript.

Competing interests The authors declare no competing interests.

Additional information
Extended data is available for this paper at https://doi.org/10.1038/s41586-018-0054-x.
Supplementary information is available for this paper at https://doi.org/10.1038/s41586-018-0054-x.
Reprints and permissions information is available at http://www.nature.com/reprints.
Correspondence and requests for materials should be addressed to S.R.W.
Publisher's note: Springer Nature remains neutral with regard to jurisdictional claims in published maps and institutional affiliations.

METHODS

Materials. Dicyclopentadiene (DCPD), 5-ethylidene-2-norbornene (ENB), second-generation Grubbs' catalyst (GC2), phenylcyclohexane, and phosphite inhibitors (TMP, TEP and TBP) were purchased from Sigma-Aldrich and used as received without further purification. For all FRPC specimens, the fibre reinforcement is Toray T300 carbon fibre 2 × 2 twill weave fabric (tow size 3,000; areal density 204 g m^{-2}). The resistive heating wire used to trigger FROMP in the manufacturing of neat resin panels and in FRPC manufacturing is a 26-gauge Kanthal wire (diameter 0.40 mm; resistivity 1.4×10^{-4} Ω cm).

Frontal polymerization. Given that DCPD is solid at room temperature, we first melt it in an oven at 35 °C and then add 5 wt.% ENB to depress the melting point. All references to DCPD herein refer to this 95/5 DCPD/ENB solution. This mixture is then degassed at 16 kPa overnight. In a typical experiment, we weigh out 3.21 mg GC2 into an Eppendorf tube and dissolve it in 400 μl phenylcyclohexane. We add an appropriate amount of phosphite inhibitor (0–14 molar equivalents with respect to GC2) to the solution via a volumetric syringe. The catalyst/inhibitor solution is then added to 5 g DCPD (10,000 molar equivalents with respect to GC2) and thoroughly mixed.

Unless otherwise specified, the solution is frontally polymerized immediately after mixing. Different types and concentrations of inhibitor are used for each manufacturing technique to tune the reaction kinetics based on the requirements of the target application. The various inhibitor concentrations and resin incubation times are summarized in Extended Data Table 1.

FROMP of stiff gel. We use TBP (2 molar equivalents with respect to GC2) as the inhibitor for the free-standing gel specimens shown in Fig. 2a–c. The solution is poured into a flat glass plate mould with a polyurethane rubber gasket and allowed to polymerize for 18 hours at room temperature. The glass plates are then carefully removed and the free-standing gel is extracted from the mould. Gels are then either deformed by hand (Fig. 2a, b) or embossed with a plastic stamp (Fig. 2c) to create the pattern. A soldering iron is used to locally heat a single point on the gel, initiating the FROMP reaction.

For micropatterned specimens (Fig. 2d, e), a patterned silicon wafer is attached to a microscope glass slide using cyanoacrylate adhesive. A second microscope slide is used with a polyurethane rubber gasket to form a small glass plate mould. The same chemistry described previously for free-standing gel experiments is used to fill the mould and the solution is allowed to polymerize for 18 hours. The gel is carefully peeled off the micropatterned surface and examined via optical microscopy to confirm pattern transfer. The gel is then suspended pattern-side down between two microscope slides and FROMP is initiated by applying a soldering iron to one end of the sample.

Front velocity and temperature measurements. We measure the peak temperature during FROMP by inserting a T-type thermocouple (TMQSS, Omega) into the liquid resin, gel or FRPC specimens before initiating FROMP. For experiments performed in cylindrical test tubes, we insert the thermocouple into the centre of the test tube to reduce heat-transfer effects at the test-tube wall. Similarly, for experiments performed in composite layups, the thermocouple is inserted at the mid-plane of the layup.

Frontal propagation is tracked with a Canon EOS 7D digital camera or an FLIR SC620 thermal infrared camera. Front velocity is extracted from the slope of the best-fit trendline for front position versus time. We identify the front position by a colour change and refractive-index mismatch in optical images, or a sharp thermal gradient in infrared images.

Rheological measurements. Isothermal rheological measurements are performed using a TA Instruments AR-G2 rheometer equipped with 25-mm-diameter parallel aluminium plates and a solvent trap. An appropriate amount of phosphite inhibitor (0–14 molar equivalents with respect to GC2) is dissolved in the monomer solution. Time-sweep measurements are performed at 23 °C with a strain of 0.1% and a frequency of 1 Hz. The gel times plotted in Fig. 4a correspond to the crossover of the storage modulus, G', and loss modulus, G'', as shown in Fig. 4b. For the shear thinning behaviour of the 3D printable DCPD ink (Extended Data Fig. 1d), viscosity and stress data are obtained in a flow sweep test with descending shear rate at a fixed temperature of −5 °C.

Heat of reaction and degree of cure analysis. We carry out DSC measurements on a TA Instruments Q20 DSC equipped with a CFL-50 cooling system. Samples are transferred into aluminium hermetic DSC pans at room temperature and sealed. The sample mass is determined using an analytical balance (XPE205, Mettler-Toledo). The mass of liquid resin samples is carefully maintained between 2 mg and 3 mg because of the highly exothermic nature of the studied reaction, as greater masses exceed the instrument's ability to maintain a consistent temperature gradient. We determine cure profiles of liquid resins and gels at temperatures between −50 °C and 250 °C with constant ramp rates. The enthalpy of reaction is determined through the integration of heat flow over the exothermic peak after baseline correction. The specific heat capacity is determined between 25 °C and 200 °C by comparison with a sapphire standard.

3D printing. A DCPD/GC2 solution containing 0.5 molar equivalents of TEP with respect to GC2 is transferred into a 3 ml syringe barrel and left to stand at 23.0 °C in an environmental test chamber (MicroClimate, Cincinnati Sub-Zero Products) for 160 minutes to allow the cross-linking of the ink mixture to form a viscous liquid. Ink in the syringe barrel is then sealed with a piston and is ready for printing. The 3D printer consists of an air-operated high pressure dispensing tool (HP 3CC, Nordson EFD) mounted on a robotic motion-controlled stage (JL2000, Robocasting Enterprises). The pressure actuation and stage motion is simultaneously controlled via custom-designed software (RoboCAD 2.0). Air is supplied from a compressed air tank (Airgas) using a customized pressure controller. The print bed consists of an aluminium plate heated by a polyimide film heater (KH-608, OMEGA) to 70 °C. Glass slides are placed on the print bed to capture the prints. The barrel housing is fitted with stainless-steel dispenser tips before printing (inner diameters between 0.25 mm and 1.55 mm; Nordson EFD). The ink barrel is inserted into the dispensing tool, then cooled down to −5 °C ± 3 °C by surrounding the dispensing tool with dry ice. A few seconds after DCPD ink is printed on the heated glass slide, the front initiates via the heated print bed. The front then propagates along the filament, following the print head during printing. The shear thinning behaviour of the gel (Extended Data Fig. 1d) is crucial for the 3D printing of free-form structures. Using DSC, we estimate the degree of cure of the unprinted ink and printed specimen to be about 23.6% and 99.2%, respectively (Extended Data Fig. 1c).

Fabrication and testing of neat resin panels. We use a resin solution containing 1 molar equivalent of TBP with respect to GC2 for the fabrication of both FROMP-pDCPD and conventionally cured pDCPD resin panels. The resin mixture is degassed for 10 minutes at 10 kPa and then poured into cell casting moulds. We use a 215.9 mm × 203.2 mm × 6.4 mm U-shaped polyurethane spacer between two glass plates for tensile testing specimens, and a 139.7 mm × 127.0 mm × 9.5 mm U-shaped polyurethane spacer between two glass plates for fracture toughness specimens. Panels are manufactured using liquid FROMP, gel FROMP, and conventional (oven) cure. Liquid FROMP panels are initiated immediately by applying an electric current to a resistive wire placed along one edge of the mould. The power supply is turned off as soon as frontal propagation is observed, and remains off for the remainder of the propagation. We keep gel FROMP panels at 23 °C for approximately 6 hours, at which time the resin becomes a rubbery gel, before initiating the FROMP via a resistive wire placed along one edge of the mould. The power supply is turned off as soon as frontal propagation is observed, and remains off for the remainder of the propagation. Conventional-cured panels are cured for 24 hours at 30 °C, 2 hours at 70 °C and 1.5 hours at 170 °C.

For comparison, we also manufacture panels of an aerospace-grade bisphenol A (BPA) epoxy resin. A solution of Araldite LY 8605 (resin) and Aradur 8605 (hardener) is mixed (100/35 weight ratio) and then degassed for 1 hour at an absolute pressure of 10 kPa. The epoxy system is poured into cell casting moulds similar to those used for the pDCPD panels. Samples are cured according to the manufacturer's recommended cure cycle, which is 24 hours at room temperature, 2 hours at 121 °C and 3 hours at 177 °C.

We cut dog-bone specimens for tensile testing from the manufactured panels following ASTM standard D638 type I dimensions. Tensile tests are conducted using an Instron 5984 with a 150 kN load cell and a video extensometer is used to measure the strain. Tests are performed at a crosshead speed of 5 mm min^{-1}. We calculate Young's moduli over a range of strains from 0.1% to 0.3%. Single-edge-notch bending (SENB) specimens for fracture toughness experiments are machined from the panels following ASTM standard D5045. Fracture toughness tests are conducted using an Instron 8841 with a 1 kN load cell. Pre-cracks are created by tapping a razor blade into the edge notch of the sample with a hammer. We measure crack lengths optically, using an optical digital microscope (VHX-5000, Keyence). A three-point bending fixture is used with a 12 cm span, and tests are conducted at a crosshead speed of 10 mm min^{-1}. We calculate K_{IC} according to the referred standard.

Fabrication and testing of composite parts. For all composite specimens, we use 12 plies of dry fabric. For FROMP-pDCPD composites, we mix 0.3 molar equivalents of TBP with respect to GC2 with the resin solution. A double-bagged VARTM technique is used to infuse the fabric with the liquid resin. To minimize heat loss during cure and to mitigate quenching of the front, we prepare the layup on a thermally insulating tool plate (448-D, Fibre Glast Developments Corp.). A low vacuum (64.3 kPa) is applied on the inner bag using a vacuum pump (2047B-02, WelchTM DryFastTM) to infuse the resin. A 1.7 kPa vacuum is applied on the outer bag using a second vacuum pump to compact the layup for producing cured parts with a high volume fraction of fibres. To initiate FROMP, we place an electrically resistive wire within the fabric stack and connect it in series to a DC power source. Once resin completely infuses the fabric stack, we apply a constant electric current across the resistive wire until FROMP initiates in the layup, and then turn the power off.

We evaluate the effect of three different curing modes on total cure time for a 10 cm × 20 cm laminate (Fig. 3a–c). For the in-plane curing modes (Fig. 3a, b), a DC power supply powers the embedded wires for 20 seconds at 19 W per wire. For the through-thickness curing mode (Fig. 3c), an AC power supply (L1010, Staco Energy Products Co.) powers the surface heater (SRFG-408/10, OMEGALUX) for 32 seconds at a maximum rating of 320 W. We use an FLIR SC620 thermal infrared camera to record the surface temperature of the layup and to measure the total cure time for each mode. Given that we carry out thermal imaging on the surface of the FRPC layup, we also embed a thermocouple inside the layup to measure the actual temperature of the FRPC during manufacturing. We found infrared readings to be lower than the actual laminate temperature by around 30 °C, owing to heat dissipation and radiation by the layup materials.

We prepare the corrugated composite panel (Fig. 2i) by stacking 12 plies of 13 cm × 23 cm fabric on a custom metal tool plate. To minimize heat loss to the thermally conductive metal tooling during cure, we preheat the entire layup to 50 °C in a convection oven before resin infusion. The layup is then removed from the oven and immediately infused with resin. Finally, FROMP is triggered using the thermal stimulus via the embedded resistive wire.

We manufacture conventionally cured pDCPD and epoxy composite panels as a control, for comparing the mechanical properties of the FROMP-cured composites. We fabricate these panels using a traditional wet-layup technique and then cure them in a hydraulic press (MTP-13, Tetrahedron) under constant applied platen force of 13.3 kN. The matrix material for the conventional-cured pDCPD-FRPCs is a resin formulation with a pot life of at least one hour (1.0 molar equivalents of TBP with respect to GC2). We use the same cure cycle as for the conventionally cured neat pDCPD panels. The matrix material and cure cycle for the epoxy composites are the same as for the neat epoxy panels described previously.

We determine the void content of the fabricated laminates by polishing the cross-sections of five to eight specimens taken from each FRPC panel, and imaging them using an optical digital microscope (VHX-5000, Keyence). These images are then analysed using ImageJ software to calculate the total void area to cross-sectional area ratios for each specimen. The void volume fraction for each panel is then taken as the average void volume fraction across the analysed specimens. The fibre volume fraction, V_f, of FRPC panels is calculated as $V_f = \frac{f_A n}{\rho_f t}$, where f_A is the areal weight of fabric, n is the number of plies, ρ_f is the fibre density and t is the average laminate thickness. The quality of different FRPC panels is summarized in Extended Data Table 2.

For the tensile tests, we tab carbon FRPC panels with G10 FR4 glass-fibre/epoxy end tabs that are 44.5 mm long, 0.20 mm thick and with a 20° taper. We roughen the surfaces of the end tabs and panels at the adjoining areas by lightly sandblasting them to increase mechanical grip, and adhere them to each other using JB Weld adhesive. The panels are then cut into tensile specimens with nominal dimensions of 203.2 mm × 12.7 mm. We test composite specimens according to ASTM standard D3039 with a crosshead speed of 2 mm min^{-1} on an Instron 5984 with a 150 kN load cell and use an Instron video extensometer to measure the strain. Young's moduli are calculated over a strain range from 0.3% to 0.6%.

Computational modelling. In an axisymmetric setting, the governing partial differential equations describing the FROMP reaction can be written as:

$$\begin{cases} \kappa\left[\dfrac{\partial^2 T}{\partial r^2} + \dfrac{1}{r}\dfrac{\partial T}{\partial r} + \dfrac{\partial^2 T}{\partial z^2}\right] + \rho H_r \dfrac{\partial \alpha}{\partial t} = \rho C_p \dfrac{\partial T}{\partial t} \\ \dfrac{\partial \alpha}{\partial t} = A \exp\left(-\dfrac{E}{RT}\right)(1-\alpha)^n \alpha^m \dfrac{1}{1+\exp[C(\alpha-\alpha_c)]}, \end{cases}$$

where T (in K) and α (non-dimensional) respectively denote the temperature and the degree of cure; κ (in W m^{-1} K^{-1}) denotes the thermal conductivity; C_p (in J kg^{-1} K^{-1}) is the specific heat; ρ (in kg m^{-3}) denotes the density; H_r (in J kg^{-1}) is the total enthalpy of the reaction; r and z (in m) are the radial and longitudinal coordinates; and t (in s) is the time. The second equation corresponds to the cure kinetics model, with A (8.55×10^{15} s^{-1}), E (110.75 kJ mol^{-1}), R (8.314 J mol^{-1} K^{-1}), n (1.7), and m (0.8) respectively denoting the pre-exponential factor, the activation energy, the universal gas constant, and two constants associated with the Prout–Tompkins model that account for the autoactivating effects. The model also includes an added diffusion factor with $C = 14.5$ and $\alpha_c = 0.4$ to describe the cure kinetics of the monomer along with the effects of diffusion[31]. We calculated the above constants by solving a nonlinear model-fitting optimization problem on the heat of reaction curves obtained by dynamic DSC experiments on a formulation containing 0.5 molar equivalents of TBP with respect to GC2 catalyst. The above governing equations are completed by the following initial and boundary conditions:

$$\begin{aligned} &T(r, z, t=0) = T_0 \\ &\alpha(0 \le r \le a, z, t=0) = \alpha_0 \\ &\{T(0 \le r \le a, z=0, t) = T_{trig} \quad 0 \le t \le t_{trig} \\ &\frac{\partial T}{\partial z}(0 \le r \le a, z=0, t) = 0 \quad t > t_{trig} \end{aligned}$$

while adiabatic conditions are imposed at all other boundaries. T_0 (23 °C) and α_0 (0.07) are respectively the initial temperature and the degree of cure of the monomer solution. T_{trig} is the trigger temperature. The physical and thermal properties used in this study are listed in Extended Data Table 3.

We conducted the numerical analysis using the Multiphysics Object-Oriented Simulation Environment (MOOSE)[32], an open source C++ finite-element solver that includes mesh adaptivity capability. The system of nonlinear partial differential equations is solved at every time step using a combination of the implicit Euler time-stepping scheme and a preconditioned Jacobian-free Newton Krylov method[33,34].

The first simulation presented in Fig. 3d involves the frontal polymerization of DCPD inside a glass tube (Extended Data Fig. 2a). The domain dimensions are length (L) = 7.5 mm, inner radius (a) = 5.5 mm and wall thickness (b) = 1 mm, with L chosen to be long enough to capture the quasi-steady-state propagation of the front. We use 151,470 four-node quadrilateral elements to discretize the domain at the beginning of the simulation, and apply a maximum refinement level of 9 to adapt the mesh in the vicinity of the advancing front. The polymerization is initiated by applying a T_{trig} of 210 °C, for a t_{trig} of 7 seconds, along the left edge of the domain (Extended Data Fig. 2a). Extended Data Fig. 2b, c depict the associated temperature contours during polymerization. The simulation yields a maximum temperature, T_{max}, of 223 °C and a velocity of the polymerization front, V, of 6.4 cm min^{-1}, in good agreement with the experimental results.

To capture the effect of a carbon-fibre tow as a conductive element on the propagation of the front, we perform a second simulation (Extended Data Fig. 2d), with tow radius (c) = 0.5 mm, and a, b and L the same as for the case without the tow. For this problem, the same mesh is used at the beginning of the simulation; however, a maximum refinement level of 12 is applied to capture the exceptionally sharp gradients associated with the large mismatch in thermal conductivities between the carbon-fibre tow and the DCPD resin ($\kappa_{CF}/\kappa_{resin} = 68.75$). The reaction is initiated by applying a T_{trig} of 210 °C, for a t_{trig} of 7 seconds. Extended Data Fig. 2e, f, which present snapshots of the temperature contours during the frontal-polymerization event, clearly shows the effect of the conductive element on the front profile. The computed front velocity is 10% higher than in the neat resin case.

Data availability. The data that support the findings of this study are available from the corresponding author on reasonable request.

Code availability. We performed the simulations using MOOSE, an open-source C++ finite-element framework developed at Idaho National Laboratory (http://mooseframework.org).

31. Yang, G. & Lee, J. K. Curing kinetics and mechanical properties of endo-dicyclopentadiene synthesized using different Grubbs' catalysts. *Ind. Eng. Chem. Res.* **53**, 3001–3011 (2014).
32. Gaston, D., Newman, C., Hansen, G. & Lebrun-Grandié, D. MOOSE: a parallel computational framework for coupled systems of nonlinear equations. *Nucl. Eng. Des.* **239**, 1768–1778 (2009).
33. Knoll, D. A. & Keyes, D. E. Jacobian-free Newton–Krylov methods: a survey of approaches and applications. *J. Comput. Phys.* **193**, 357–397 (2004).
34. Pernice, M. & Walker, H. NITSOL: a Newton iterative solver for nonlinear systems. *SIAM J. Sci. Comput.* **19**, 302–318 (1998).

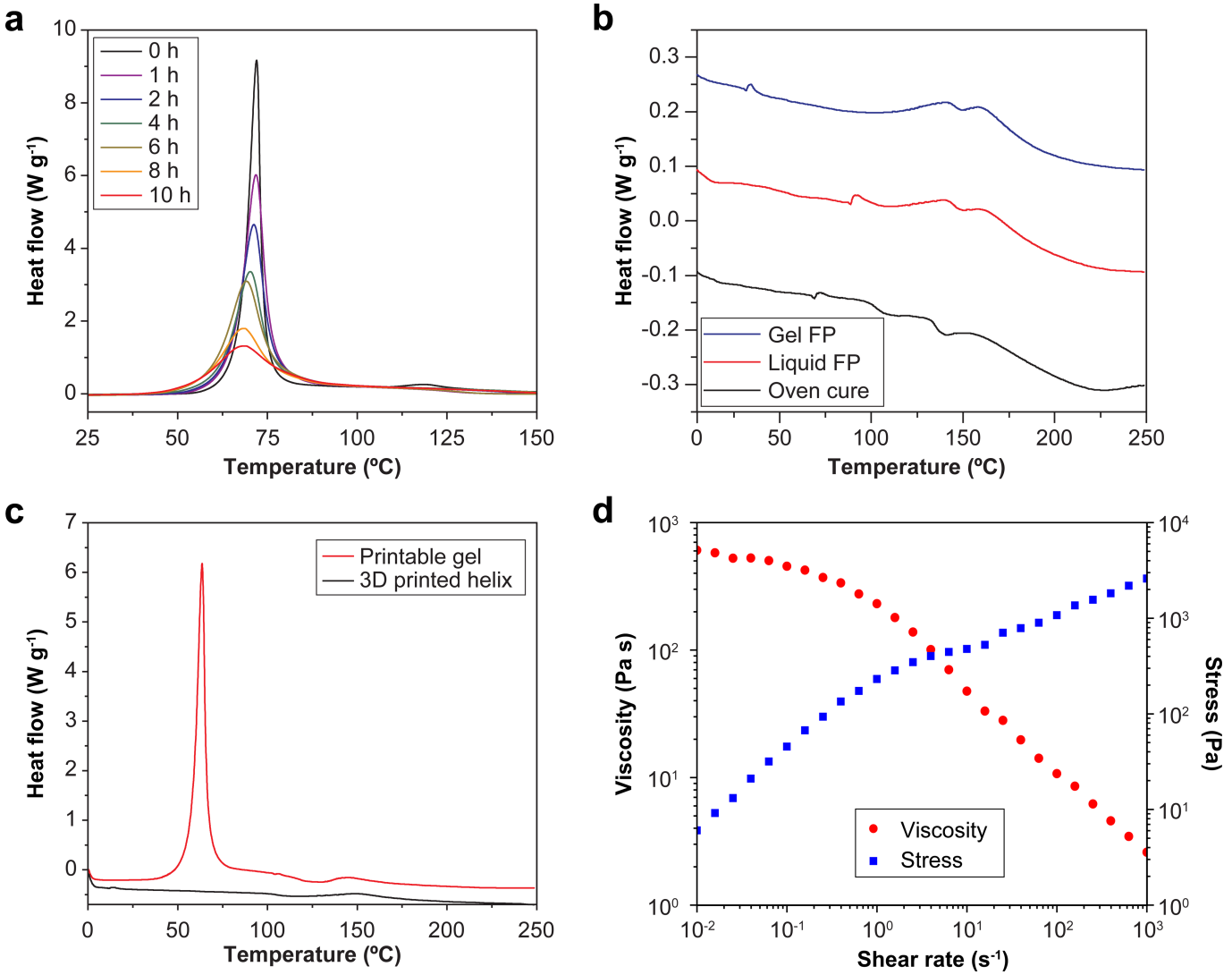

Extended Data Fig. 1 | Characterization of DCPD gel and pDCPD products. a, Heat of reaction, measured by DSC, for the formulation presented in Fig. 4b after ageing the resin at 23 °C for the indicated times. As the curing proceeds, the exothermic peak shifts slightly to lower temperatures and broadens. **b**, Heat of reaction of pDCPD specimens produced by liquid FROMP, gel FROMP and conventional (oven) cure approaches, indicating fully cured products with a degree of cure of 99.6%, 99.6% and 99.7%, respectively. **c**, Heat of reaction of the gel before 3D printing and of a cured part after printing, measured by DSC. There is minimal heat of reaction in the printed polymer, indicating a 99.2% degree of cure. **d**, Rheological profile of the 3D printable gel, showing shear thinning behaviour.

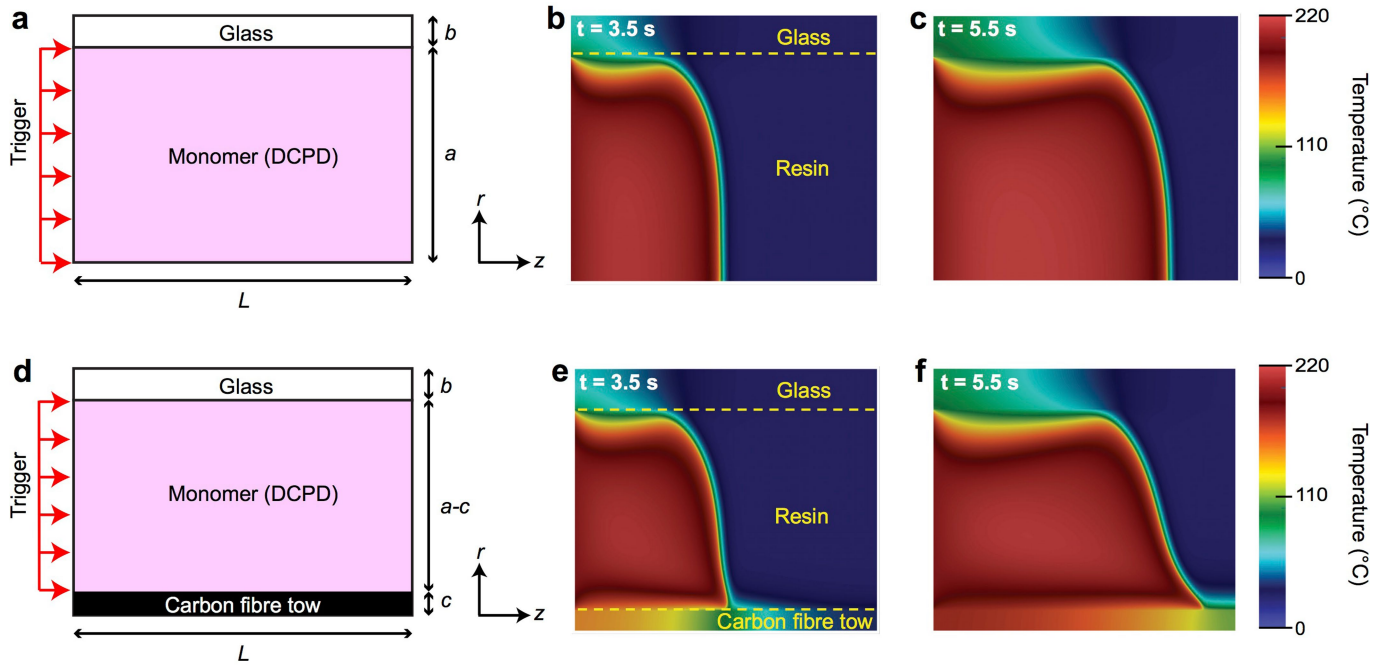

Extended Data Fig. 2 | Simulation of FROMP reaction. a, Schematic representation of the axisymmetric model of FROMP in a glass tube. **b**, **c**, Propagation of the reaction front in neat resin. **d**, Schematic representation of the axisymmetric model of FROMP in the presence of a carbon-fibre tow placed at the centre of the glass tube. **e**, **f**, Evolution of the location and profile of the polymerization front in the presence of a carbon-fibre tow.

Extended Data Table 1 | Inhibitor concentration and resin incubation time for different manufacturing techniques and the corresponding front temperature and velocity

Manufacturing technique	Inhibitor type	Inhibitor concentration (molar equiv. to GC2)	Resin incubation time	Front temperature* (°C)	Front velocity* (cm min^{-1})
Liquid resin (gel time measurements)	TMP, TEP, TBP	0-14	< 1 min	~ 215 (0.3-1 equiv.) ~ 200 (2-4 equiv.) ~ 175 (8 equiv.)†	See Fig. 4a
Stiff gel FROMP	TBP	2	18 h @ room temp.	145	3.6
3D printing	TEP	0.5	160 min @ 23.0 °C	170‡	9.6
FROMP-pDCPD neat panel (liquid FROMP)	TBP	1	< 1 min	216	6.8
FROMP-pDCPD neat panel (gel FROMP)	TBP	1	6 h	184	5.7
Conventional-cured pDCPD neat panel	TBP	1	< 1 min	N/A	N/A
FROMP-pDCPD FRPC	TBP	0.3	< 5 min	138	9.8
Conventional-cured pDCPD FRPC	TBP	1	< 5 min	N/A	N/A

TMP: trimethyl phosphite; TEP: triethyl phosphite; TBP: tributyl phosphite.
*Front temperatures and velocities are highly dependent on the material and geometrical conditions used for each manufacturing technique. The values reported here correspond to the exact experimental conditions described in the Methods section.
†Front temperatures for a given concentration of phosphite inhibitor are similar regardless of the identity of the inhibitor.
‡The front temperature of the 3D printed filament is recorded using a thermal infrared camera, however, it is difficult to determine the exact temperature of the front due to the low distance between the heated substrate and printed material.

Extended Data Table 2 | Comparison of FRPC panels made with different manufacturing techniques

Manufacturing technique	Void content (%)	V_f (%)	Degree of cure (%)
FROMP-pDCPD FRPC	0.15 ± 0.20	51.3 ± 1.0	80.5 ± 3.9
Conventional-cured pDCPD FRPC	1.30 ± 0.56	51.1 ± 1.3	89.6 ± 1.3
Conventional-cured epoxy FRPC	0.25 ± 0.15	52.2 ± 1.2	98.8 ± 1.7

Extended Data Table 3 | Physical and thermal properties of the various components used in computational modelling

	κ (W m^{-1} K^{-1})	ρ (kg m^{-3})	H_r (J g^{-1})	C_p (J kg^{-1} K^{-1})
Monomer	0.15	980	350	1,600
Carbon fibre	10.45	1,760	_	795
Glass	1.14	2,230	_	800